Journal of
Manufacturing and Materials Processing

MDPI

Article

Using Coatings Based on the ZrN System to Improve the Corrosion Resistance of Stainless Steel Products

Sergey Grigoriev [1], Marina Volosova [1], Valery Zhylinski [2], Catherine Sotova [1], Filipp Milovich [3], Alexander Kalinichenko [2], Abdelhafed Taleb [4], Elena Eganova [5], Tatyana Borovik [1] and Alexey Vereschaka [6,*]

[1] Department of High-Efficiency Machining Technologies, Moscow State Technological University «STANKIN», Vadkovsky per. 1, Moscow 127994, Russia; s.grigoriev@stankin.ru (S.G.); volosova1978marina@yandex.ru (M.V.); e.sotova@stankin.ru (C.S.); tanuwka2004@yandex.ru (T.B.)
[2] Department of Chemistry, Technology of Electrochemical Production and Electronic Engineering Materials, Chemical Technology and Engineering Faculty, Belarusian State Technological University, 13a, Sverdlov Street, 220006 Minsk, Belarus; zhilinski@yandex.ru (V.Z.); ask0708@mail.ru (A.K.)
[3] Materials Science and Metallurgy Shared Use Research and Development Center, National University of Science and Technology "MISiS", Leninsky Prospect 4, Moscow 119049, Russia; filippmilovich@mail.ru
[4] Institut de Recherche de Chimie Paris, Sorbonne Université, 4 Place Jussieu, 75231 Paris, France; abdelhafed.taleb@sorbonne.universite.fr
[5] Institute of Nanotechnology of Microelectronics, Russian Academy of Sciences INME RAS, Leninskiy Prospect 32A, Moscow 119334, Russia; eganova.e@inme-ras.ru
[6] Institute of Design and Technological Informatics of the Russian Academy of Sciences (IDTI RAS), Vadkovsky per. 18-1a, Moscow 127994, Russia
* Correspondence: dr.a.veres@yandex.ru

Abstract

This article investigates the anticorrosive properties of Zr-ZrN coatings, including Zr-(Zr,Hf)N, Zr-(Zr,Ti)N, Zr,Hf-(Zr,Hf,Nb)N, and Zr,Nb-(Zr,Nb)N, deposited on AISI 321 stainless steel substrates. The hardness and elasticity modulus of these coatings, as well as their scratch test strength, were measured. Corrosion current densities were calculated using the polarisation resistance method and by extrapolating the linear sections of the cathodic and anodic curves under electrode polarisation. The structure and composition of the sample surfaces were analysed by transmission electron microscopy. Notably, the nitride coatings reduced the corrosion current density in a 3% aqueous NaCl solution at 25 °C by more than 10 times, from 6.96 for the uncoated substrate to 0.17 μA/cm^2 for the Zr-(Zr,Ti)N-coated sample. The addition of Ti nitride to Zr-ZrN led to the most significant decrease in the corrosion current density. However, the introduction of Nb caused an increase in the corrosion rate and a decrease in the polarisation resistance, and Hf did not affect the corrosion-protective properties of the studied nitride coatings.

Keywords: anticorrosive properties; coating; zirconium nitride

Academic Editor: Zhixing Guo

Received: 14 October 2025
Revised: 3 November 2025
Accepted: 8 November 2025
Published: 10 November 2025

Citation: Grigoriev, S.; Volosova, M.; Zhylinski, V.; Sotova, C.; Milovich, F.; Kalinichenko, A.; Taleb, A.; Eganova, E.; Borovik, T.; Vereschaka, A. Using Coatings Based on the ZrN System to Improve the Corrosion Resistance of Stainless Steel Products. *J. Manuf. Mater. Process.* **2025**, *9*, 369. https://doi.org/10.3390/jmmp9110369

1. Introduction

Nitride coatings have been employed to improve the corrosion resistance of stainless steel since at least the early 1990s. In particular, the corrosion resistance of austenitic steel was markedly increased by depositing TiN and ZrN coatings [1]. In the case of ZrN, the highest corrosion resistance was achieved using alternating layers of Zr and ZrN. The corrosion resistance of TiN and ZrN coatings on an AISI 304 stainless steel substrate in a 0.5 N NaCl solution has also been investigated [2], showing that TiN is inert, whereas ZrN reacts with an aggressive environment. The authors suggested that the nitrogen (N) in ZrN is replaced by oxygen (O), forming a zirconium oxide (ZrO_2) film, which has

good corrosion resistance and improves corrosion protection. ZrO_2 forms spontaneously upon contact with an O-containing environment, occurring naturally during the coating deposition process. The inclusion of a ZrO_2 layer in the coating structure reduces the corrosion current density in 3.5 wt.% NaCl and 20 wt.% HCl solutions compared with a ZrN coating without an oxide layer [3]. The anticorrosive properties of the multilayer coating are attributed to a combined effect, including increased strength and reduced stress levels owing to the multilayer structure and high corrosion resistance provided by the ZrO_2 sublayer. Compared with the uncoated sample, the corrosion current density (i_{corr}) and polarisation current density (i_p) values for samples with ZrN/Zr bilayers were significantly lower (at least one order of magnitude) than those measured for samples with a single Zr or ZrN coating [4]. This result was ascribed to a decrease in the density of point defects in coatings with a multilayer structure. The interlayer interface inhibits the corrosion channel from passing through the coatings into the metal substrate, minimising the area of impact and, thus, improving corrosion resistance.

TiN and ZrN coatings were shown to significantly enhance the corrosion resistance of 316L stainless steel [5]. Electrochemical impedance spectroscopy and polarisation curves showed that the TiN coating had higher corrosion resistance than the ZrN coating. At the same time, a comparison of the anticorrosion properties among TiN, CrN, and ZrN coatings showed that ZrN provided the strongest corrosion protection, whereas TiN only outperformed the uncoated samples [6]. To further reduce corrosion, coatings combining TiN and ZrN have also been employed. TiN/ZrN coating with a nanocomposite structure improved the corrosion resistance by approximately 6 times compared with the uncoated sample [7]. This coating also increased the corrosion potential from −0.085 to 0.080 V, which significantly exceeds the results obtained for monolithic CrN and TiN coatings. The corrosion properties of nanocrystalline (Ti,Zr)N coatings on an AISI 304 stainless steel substrate were also studied [8]. The steady-state potential during the corrosion process (E_{corr}) only slightly differs for the coated and uncoated samples. This may indicate that the corrosion of the TiN- or (Ti,Zr)N-coated samples was mainly caused by the dissolution of the metal substrate, and not directly by the TiN or (Ti,Zr)N coatings. At the same time, TiN and (Ti,Zr)N coatings significantly reduce the i_{corr} values compared with uncoated samples.

The coating structure also has a significant effect on its corrosion resistance. Single-layer, multilayer, and gradient ZrN coatings were shown to reduce i_{corr} by 83.0%, 99.8%, and 95.8%, respectively [9]. Thus, the use of gradient and multilayer coating structures can enhance corrosion resistance by increasing the crack resistance and mitigating the formation of penetration channels. The coating structure can be modified by introducing additional elements, such as silicon (Si). A nanocomposite coating (Zr,Si)N, in which the nanoscale crystallised ZrN phase is embedded in an amorphous silicon nitride matrix, was used to improve the corrosion resistance of stainless steel in a 3.5% NaCl solution [10]. The results showed that (Zr,Si)N coatings are more uniform than ZrN and exhibit higher corrosion resistance than ZrN and the uncoated sample. ZrN-coated steel exhibited localised corrosion through pores in the coating, whereas (Zr,Si)N-coated steel exhibited uniform corrosion at the coating–steel interface [11].

An additional increase in corrosion resistance can be achieved by optimising the deposition parameters. For instance, the nitrogen gas (N_2) pressure has a significant effect on corrosion resistance because of the changes in coating defects [12]. The ZrN coating deposited on a 316 L steel substrate at an optimal N_2 pressure (3.5 Pa) demonstrated increased corrosion resistance (E_{corr} = 0.307 V, i_{corr} = 2.085 × 10^{-7} A/cm^2), and the coating structure exhibited minimal defects. The effect of substrate bias voltage on the corrosion properties of the ZrN coating was also studied [13]. Additional post-treatment of the coated samples, such as vacuum annealing, also enables further improvements in corrosion

resistance. For example, the corrosion resistance of vacuum-annealed 304SS steel with a ZrN coating in a NaCl solution increased by at least 100 times compared with that of uncoated samples [14]. Multilayer nanostructured ZrN/CrN coatings provided a significant increase in resistance to aggressive environments, owing to the enhanced barrier properties of multilayer structures [15,16]. Similarly, multilayer (Cr,Zr)N/ZrN coatings exhibited more effective anticorrosion properties than single-layer (Cr,Zr)N and ZrN coatings [17]. For multilayer (Cr,Zr)N/ZrN coatings, i_{corr} was only 2.078 × 10^{-7} A/cm^2, 2 times lower than that of the single-layer (Cr,Zr)N coating. The multilayer coating with local coherent interfaces appears to be beneficial. The ratio of the nanolayer coating thicknesses also affects the corrosion resistance. Potentiodynamic polarisation tests showed that multilayer CrN/ZrN and CrN/(Cr,Al)N coatings significantly improve the corrosion resistance of stainless steel [18]. Moreover, the CrN/ZrN coating demonstrated the lowest corrosion current density because it had a lower defect density and higher chemical stability than the CrN/(Cr,Al)N coating. Multilayer CrN/ZrN coatings (with different modulation periods of 1, 8, 15, and 30) were applied to AISI 420 steel substrates [19].

The corrosion properties of NbN-based coatings have also been actively studied. In particular, multilayer TiN/NbN coatings provided more corrosion protection than single-layer TiN and NbN coatings [20–22]. The corrosion resistance of multilayer coatings improved with an increase in the total number of interfaces in the coatings. Furthermore, effective corrosion protection was provided using CrN/NbN coatings with a nanolayer structure [23]. Electrochemical corrosion testing revealed that the corrosion resistance of the NbN coating tended to increase with increasing spray power [24]. Multilayer CrN/NbN coatings demonstrated a low corrosion rate in 3.5% NaCl solutions and effectively protected the steel substrate from corrosion [25–27]. Nanolayer CrN/NbN coatings showed distinct passivation behaviour, with pitting potentials ranging from 230 to 400 mV, depending on their chemical composition and residual stress level [28]. The defect rate in CrN/NbN coatings decreased, and the corrosion resistance increased, with increasing bias voltage and substrate surface temperature [29].

An investigation of (Nb,Al)N coatings with different Al contents showed that the addition of Al negatively affects the corrosion resistance [30,31]. Substrates with a CrN/NbN coating showed higher corrosion resistance than substrates with a (Cr,Al,Ti)N coating [32]. Moreover, the introduction of 40 or 60 at.% Al increased the coating resistance to corrosion in a 3.5% NaCl solution, owing to the formation of $Al(OH)_3$ and Nb_2O_5 films.

HfN-based coatings are also effective in corrosion protection [33]. A multilayer Hf/HfN and HfN/VN coating exhibited low corrosion current density and a small number of corrosion pits after salt spray test [34,35]. The corrosion current density of samples with (Hf,Y)N coatings (9.8 to 18.5 at.% Y) decreased by two orders of magnitude compared with that of the substrate, reaching a minimum of 4.21 × 10^{-8} A/cm^2 [36].

Overall, it can be concluded that ZrN-, NbN-, and HfN-based coatings can improve the corrosion resistance of stainless steel surfaces. The introduction of additional elements and the use of multilayer coating structures are generally effective for further improving the corrosion resistance. However, the introduction of some elements, such as Al, into the coating composition can negatively impact its corrosion resistance.

The present article considers the corrosion properties of stainless steel specimens with (Zr,Nb)N, (Zr,Hf)N, and (Zr,Nb,Hf)N coatings. Samples with and without ZrN and (Zr,Ti)N coatings are also considered for comparison. A previous comparison of Ti6Al-4V alloy specimens with the aforementioned coatings showed the particular effectiveness of the (Zr,Hf)N coating in reducing corrosion [37]. The introduction of Hf into ZrN suppressed the corrosion rate in 3% NaCl to 0.118 μA/cm^2, whereas the addition of Nb to the ZrN system accelerated corrosion (3.440 μA/cm^2).

It is necessary to account for the significant differences in the corrosion processes that are characteristic of titanium alloys and stainless steel. Titanium alloys, such as Ti6Al-4V, are characterised by inherently high corrosion resistance in 0.9% and 3.0% NaCl solutions, which is due to the formation of a dense non-conducting oxide film on the titanium alloy surface [38–41]. Conversely, the corrosion resistance of stainless steels in these environments is related to the surface self-passivation that occurs upon contact with a corrosive environment. In this case, the transition of the stainless steel surface to a passive state is accompanied by etching of the iron (Fe) component, and the remaining chromium (Cr; more than 12 at.%) and nickel (Ni; more than 9 at.%) quickly form a dense layer that prevents the onset and spread of corrosion [42]. Hence, the corrosion resistance of stainless steel is determined not by the chemical resistance of the main elemental component, as in titanium alloys, but by the content of alloying components (Cr and Ni). Moreover, unlike titanium alloys, many stainless steels require special treatment in oxidising environments to impart their passive state [43].

The objective of this work is to increase the resistance to corrosion in sea water and wear resistance of stainless steel products operating under conditions of simultaneous exposure to corrosion and mechanical wear.

2. Materials and Methods

2.1. Coating Deposition

Samples are cylindrical in shape, 25 mm in diameter and 3 mm in thickness.

Coating deposition was performed using a VIT-2 vacuum plasma system (IDTI RAS—MSUT, STANKIN, Moscow, Russia), as previously described [44–49]. Evaporators implementing controlled accelerated arc technology [50–52] were used. This technology allows for reduced energy consumption and minimises the number of microparticles in the plasma flow.

Before coating deposition, the samples were prepared as follows:

- Rinsing in an alkaline solution at 80 °C under ultrasonication.
- Rinsing in specially purified water (filtration on a carbon filter).
- Blowing with a stream of purified air (filtration).

During deposition, the arc currents of the titanium (Ti) and zirconium (Zr) cathodes were 75 and 80 A, respectively. The arc current of the Zr (99.98%), Ti (99.97%), Zr-Nb (1:1), and Zr-Hf (1:1) cathodes was 65, 70, 85, and 90 A, respectively. The remaining parameters were the same for all processes: N_2 pressure of 0.42 Pa, substrate voltage of 150 V, tool rotation speed of 0.7 rpm, and substrate temperature maintained in the range of 400–450 °C.

2.2. Coating Properties

The surface morphology and structure of the coatings were examined by scanning electron microscopy (SEM; EVO 50, Carl Zeiss, Oberkochen, Germany), energy-dispersive X-ray spectroscopy (EDX; X-Max 80 mm^2, OXFORD Instruments, High Wycombe, UK), and transmission electron microscopy (TEM; JEM 2100, JEOL, Akishima, Japan). The elemental composition was evaluated by TEM-EDX (INCA Energy, OXFORD Instruments, High Wycombe, UK). Samples were prepared for TEM analysis by focused ion beam milling using a Strata 205 device (FEI, Hillsboro, OR, USA). Phase analysis was performed on an X-ray diffractometer (XRD)–D2 Phaser 2 Gen. (Bruker, Billerica, MA, USA). Hardness and elastic modulus were measured using an SV-500 nanotester (Nanovea, Irvine, CA, USA) and a Berkovich indenter at a maximum load of 200 mN. Average values were determined based on 20 measurements. Scratch testing was conducted using an SV-500 tester (Nanovea, Irvine, CA, USA) according to the ASTM C1624-05 standard [53].

Corrosion studies were conducted using an AUTOLAB PGSTAT302 N potentiostat-galvanostat (Metrohm Autolab B.V., Herisau, Switzerland) in a 3% NaCl solution at 25 °C, employing a three-electrode electrochemical cell with a platinum auxiliary electrode and a saturated silver chloride reference electrode. The intended operating environment is seawater. The salinity of the World Ocean averages 3.47%; in fresher seas (such as the Black Sea or the Sea of Azov), salinity is lower (approximately 1.5–2.0%), meaning 3% NaCl solution simulates seawater well. Potential values were converted to the standard hydrogen electrode scale. The working electrode area was 1 cm^2. The open circuit potential (ECP) was assessed for 1 h before potentiodynamic studies were performed. The susceptibility of samples to corrosion was assessed based on the potentiodynamic curves; the potential sweep rate was V_p = 1 mV/s, performed at an electrode polarisation (η) of ±800 mV [38], which was determined using the following formula:

$$\eta = E - E_{corr}, \quad (1)$$

where E is the electrode potential under an applied current, and E_{corr} is the steady-state potential for the corrosion process. The sample was held in 3% NaCl at 25 °C for 1 h before measurement. Corrosion current densities were calculated using Nova 2.0 software (Netherlands) and the polarisation resistance method, for experimental data obtained at low polarisations (η = ±20 mV):

$$\eta \approx \frac{RT}{nF}\frac{i}{i_0} = R_0 i \quad (2)$$

where $R_0 = \frac{RT}{i_0 nF}$ is the charge transfer resistance, Ω [42].

Additionally, all obtained potentiodynamic curves were analysed using Nova 2.0 (Netherlands) by extrapolating the linear sections of the cathodic and anodic curves with an electrode polarisation of ±100 mV from the Tafel equation:

$$\eta = a + b\, lgi_{corr} \quad (3)$$

where $a = \frac{nF}{RT}$ $\lg i_o n$ and $b = \frac{nF}{RT}$ are Tafel coefficients, B and B/decade, respectively; i_{corr} is the corrosion current density, A/cm^2; R is the universal gas constant, 8.314 J/(mol·K); T is the absolute temperature, K; F is the Faraday constant, 96.485.33 C/mol; i_o is the exchange current density, A/cm^2; and n is the number of electrons participating in the reaction [54].

Corrosion tests were carried out in a 3.0 wt.% aqueous NaCl solution at a temperature of 25 °C for 7 days. Three independent experiments were conducted for each coating type. The spread of values for certain parameters was within 17%. The final tables show the average values from the three tests.

3. Results

3.1. Substrate Properties

AISI 321 is an austenitic-ferritic stainless steel. The elemental composition of the steel is presented in Table 1.

AISI 321 is an austenitic-ferritic stainless steel. X-ray diffraction (XRD) reveals that uncoated samples contain two phases: austenite (Fm3m, A1) and ferrite or alpha-iron (Im3m, A2), in approximately equal amounts. This is consistent with the selected area electron diffraction (SAED) data (Figure 1). Austenite is stabilised by Ni because it is a high-temperature phase. Judging by the intensities of the XRD peaks, the original sample contains slightly more alpha-iron than the sample observed after corrosion testing.

Table 1. Elemental composition of AISI 321 steel.

Element	Mass Fraction (%)
Si	Max 1.0
C	Max 0.08
P	Max 0.045
Mn	Max 2.0
Cr	17–19
S	Max 0.03
Ni	9–11
Ti	0.5
Fe	Rest

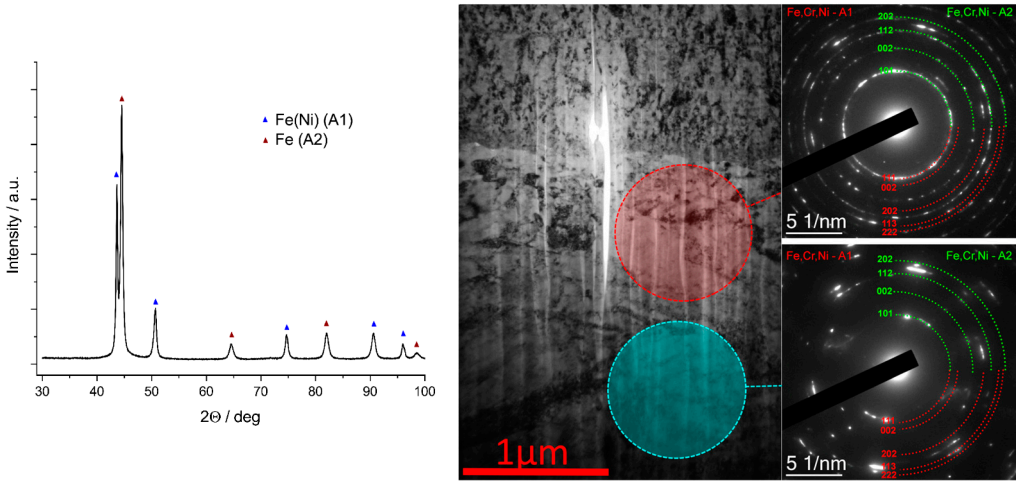

Figure 1. Phase analysis of an uncoated AISI 321 steel sample: (**a**) XRD and (**b**) SAED.

3.2. Mechanical Properties of the Coatings

The general appearance of the samples with coatings is shown in Figure 2. The samples have a colour that is characteristic of these types of coatings.

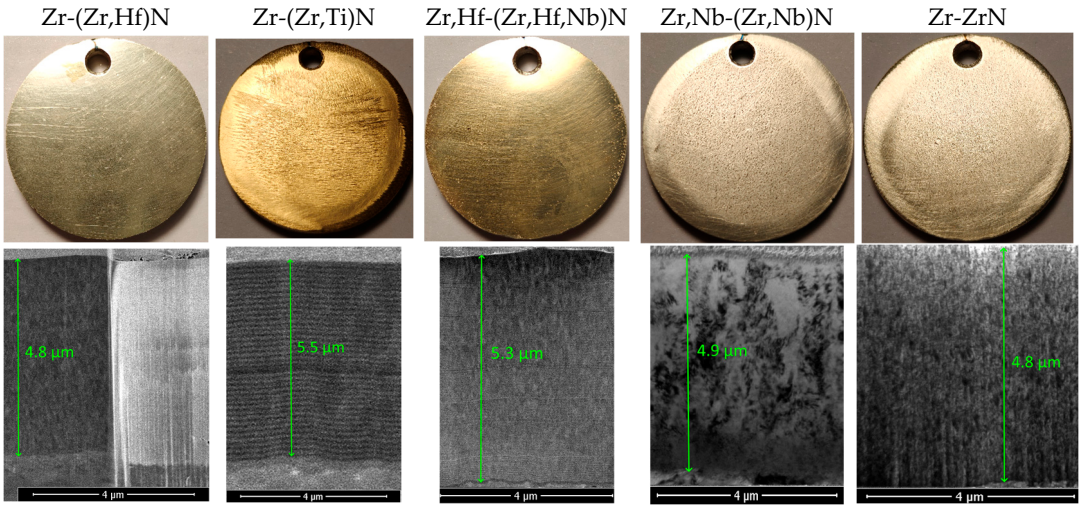

Figure 2. Surface appearance of AISI 321 steel samples with different nitride coatings (**top**), structure and thickness of coatings (**bottom**).

The coating thickness measured on the transverse section is 4.8–5.5 μm; a certain variation in thickness is typical for coatings deposited by the PVD method.

Table 2 presents the main characteristics of the coatings. In terms of composition, deposition using two cathodes of single-element composition (Zr and Ti) and a two-component Zr-Nb cathode (1:1) results in coatings with nearly equivalent (1:1) compositions, but in the case of a Zr-Hf cathode, although the elemental ratio in the cathode composition is 1:1, the coating composition is dominated by Zr with a significantly lower content of hafnium (Hf). This likely occurs because the atomic weight of Hf is significantly higher than that of Zr (178.49 and 91.224 g/mol, respectively [55]). Hf atoms require more energy to reach the substrate surface, so some of them are deposited on the chamber walls and the tooling, whereas lighter Zr atoms reach the substrate in greater quantities. A similar process occurs for the (Zr,Nb,Hf)N coating deposited using Zr-Hf (1:1) and Zr-Nb (1:1) cathodes. The (Zr,Hf)N coating exhibits the highest hardness, and the (Zr,Nb)N coating exhibits the lowest hardness. The (Zr,Nb)N coating, however, demonstrated the highest adhesion strength to the substrate (i.e., the highest total coating failure rate, L_{C2}), and the ZrN coating also demonstrated relatively high L_{C2} values. The other coatings demonstrated relatively low adhesion strengths. Note that this relatively low adhesion strength (measured using a scratch test) is due to both the large difference in the hardness of the coating and the substrate, as well as the use of a "realistic" substrate (without special surface treatment, such as polishing). These substrate properties were selected to accurately represent the operating conditions of real products in a seawater environment.

Table 2. Main characteristics of the studied coatings.

Coating	Elemental Composition [at.%]				Hardness	Adhesion Strength to the Substrate, L_{C2} (N)
	Zr	Nb	Hf	Ti		
(Zr,Nb)N	50.5	49.5	–	–	HV 2336 ± 115	15 ± 2
ZrN	100	–	–	–	HV 2993 ± 145	12 ± 2
(Zr,Hf)N	76.12	–	23.88	–	HV 3350 ± 120	7 ± 1
(Zr,Ti)N	46.58	–	–	53.42	HV 2727 ± 86	6 ± 2
(Zr,Nb,Hf)N	72.07	24.87	3.05	–	HV 2860 ± 95	6 ± 1

A previous study on steel samples with similar coatings showed that the highest wear resistance obtained during ball-on-disk testing was provided by a Zr,Hf-(Zr,Hf,Nb)N coating (wear was 1.5 times lower than that of the uncoated sample) [56]. This coating also provided the greatest reduction in the coefficient of friction.

3.3. Corrosion Behaviour of the Samples with Nitride Coatings

Polarisation studies of the corrosion behaviour of nitride coatings on the surface of AISI 321 steel were carried out by recording the anodic and cathodic polarisation curves for each sample in 3% NaCl at 25 °C (Figure 3). The general appearance of the anodic curve of an uncoated AISI 321 steel sample in 3% NaCl at 25 °C suggests the self-passivation of this steel in an oxygen-containing environment [40]. The anodic curve for AISI 321 steel in 3% NaCl displays a dissolution region from −0.77 to −0.29 V and a passivation region (−0.29 to 0.00 V). With a further increase in potential, a sharp increase in current density is observed on the anodic curve (Figure 3), which is characteristic of oxygen evolution and substrate dissolution [57].

The application of Zr-ZrN, Zr,Nb-(Zr,Nb)N, Zr-(Zr,Hf)N, Zr,Hf-(Zr,Hf,Nb)N, and Zr-(Zr,Ti)N coatings with a thickness of ~3 μm shifts the corrosion potential by 0.20–0.25 V to a more electropositive region (Figure 3). This indicates an active interaction between the coatings and the corrosive environment, involving the formation of oxonitrile layers with

increased electrical resistance [39,44]. Moreover, the passivation region that is characteristic of uncoated AISI 321 steel disappears in the anodic polarisation curves of all coated samples, which further indicates the blocking of the corrosive dissolution process of AISI 321 steel.

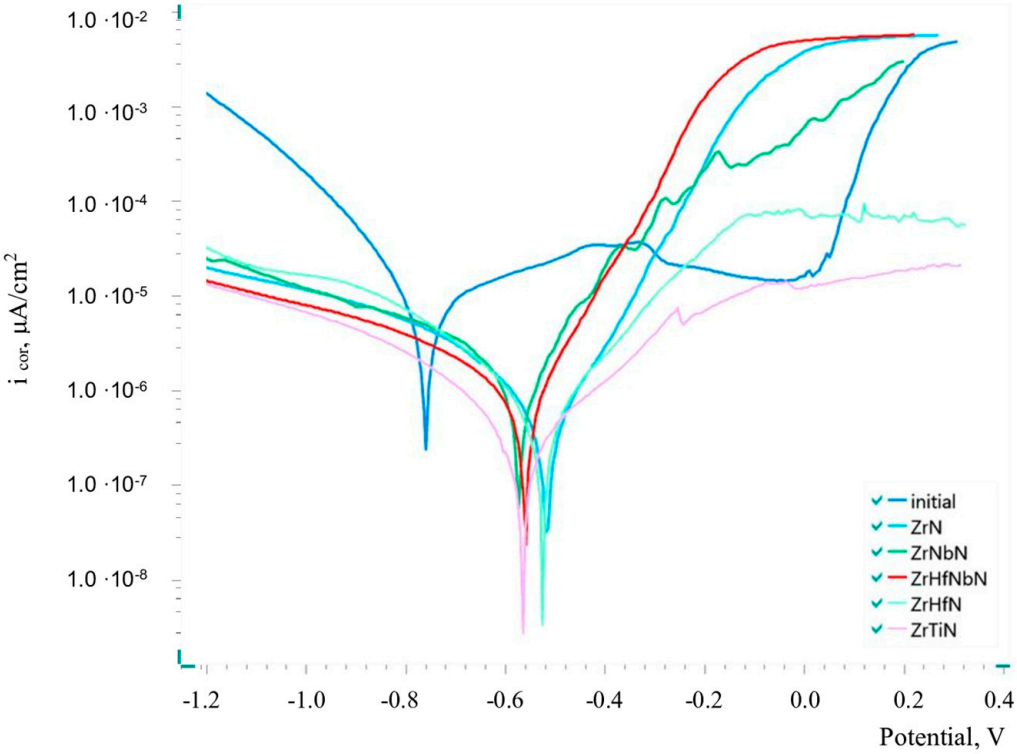

Figure 3. Superposition of the potentiodynamic curves obtained for AISI 321 steel samples with different nitride coatings in a 3% aqueous NaCl solution at 25 °C (V_p = 1 mV/s).

A comparison of the values of open circuit potentials (E_{oc}, V) for samples of AISI 321 steel with Zr-ZrN, Zr,Nb-(Zr,Nb)N, Zr,Hf-(Zr,Hf,Nb)N coatings with their corrosion potentials (E_{corr}) (Tables 3 and 4) demonstrates a shift to a more electropositive region of E_{oc} in relation to the E_{corr} value by 0.013–0.021 V, which indicates the occurrence of self-hazardization processes of the surface during the exposure of these coatings to 3% NaCl for 1 h at 25 °C. For the samples with Zr-(Zr,Hf)N and Zr-(Zr,Ti)N coatings, the value of E_{oc} is lower than E_{corr} by 0.049 and 0.079 V, respectively, which is explained by the absence of oxide films before the start of testing after 1 h of exposure in 3% NaCl at 25 °C. It should be noted that E_{oc} for the uncoated sample of AISI 321 steel is shifted by 0.267 toward a more electropositive region with respect to E_{corr}, which indicates self-passivation of this alloy in 3% NaCl at 25 °C.

Table 3. Corrosion properties extrapolated from the linear sections of the anodic and cathodic polarisation curves, obtained for AISI 321 steel samples with different coatings in 3% NaCl at 25 °C.

№	Coating	E_{oc}, V	E_{corr}, V	Tafel Plot Extrapolation Method					
				i_{corr}, μA/cm^2	P, μm/year	βc, V/dec	βa, V/dec	$E_{corr\ calc}$, V	R_0, kΩ
1	uncoated	−0.492	−0.759	6.96	80.8	0.15	0.45	−0.767	6.9
3	Zr-ZrN	−0.529	−0.516	0.25	2.9	0.11	0.11	−0.519	98.0
4	Zr,Nb-(Zr,Nb)N	−0.599	−0.571	0.78	9.1	0.19	0.11	−0.565	39.6
8	Zr-(Zr,Hf)N	−0.474	−0.523	0.31	3.6	0.15	0.12	−0.517	94.6
9	Zr,Hf-(Zr,Hf,Nb)N	−0.578	−0.559	0.45	5.2	0.16	0.10	−0.562	61.9
10	Zr-(Zr,Ti)N	−0.484	−0.563	0.16	1.9	0.15	0.16	−0.563	207.0

Table 4. Polarisation resistance determined from the corrosion potential region, obtained for AISI 321 steel samples with different coatings in 3% NaCl at 25 °C.

№	Coating	E_{corr}, V	Polarisation Resistance Method		
			i_{corr}, μA/cm^2	P, μm/year	R_0, kΩ cm^2
1	uncoated	−0.759	4.77	55.4	5.5
3	Zr-ZrN	−0.516	0.34	3.9	77.8
4	Zr,Nb-(Zr,Nb)N	−0.571	0.84	9.7	31.1
8	Zr-(Zr,Hf)N	−0.523	0.34	3.9	76.9
9	Zr,Hf-(Zr,Hf,Nb)N	−0.559	0.57	6.6	45.8
10	Zr-(Zr,Ti)N	−0.563	0.17	2.0	154.4

Taking into account the minimum corrosion currents observed at the corrosion potential in a 3% aqueous NaCl solution at 25 °C for both the coated uncoated AISI 321 steel samples, the polarisation resistance was determined from the corrosion potential region (Table 3), and the corrosion current density was estimated by extrapolating the linear sections of the anodic and cathodic polarisation curves (Table 4).

Note that the current density values for AISI 321 steel coated with Zr-ZrN, Zr,Nb-(Zr,Nb)N, Zr-(Zr,Hf)N, Zr,Hf-(Zr,Hf,Nb)N, and Zr-(Zr,Ti)N, as calculated by extrapolating the Tafel sections of the anodic and cathodic polarisation curves (Table 3), are within the range of 0.17–0.84 μA/cm^2, which are somewhat higher than the current density values calculated based on the polarisation resistance in the corrosion potential region (Table 4). This indicates that the method of determining the polarisation resistance for nitride coatings is more adequate for assessing the corrosion rate [38,57].

The polarisation resistance values of the coated samples during the corrosion process are in the range of 31.1–154.4 kΩ cm^2. A comparison of the current density and polarisation resistance (Figure 4) reveals a discrepancy of 3–27%, which largely reflects the general error of electrochemical methods for assessing corrosion resistance [38,57].

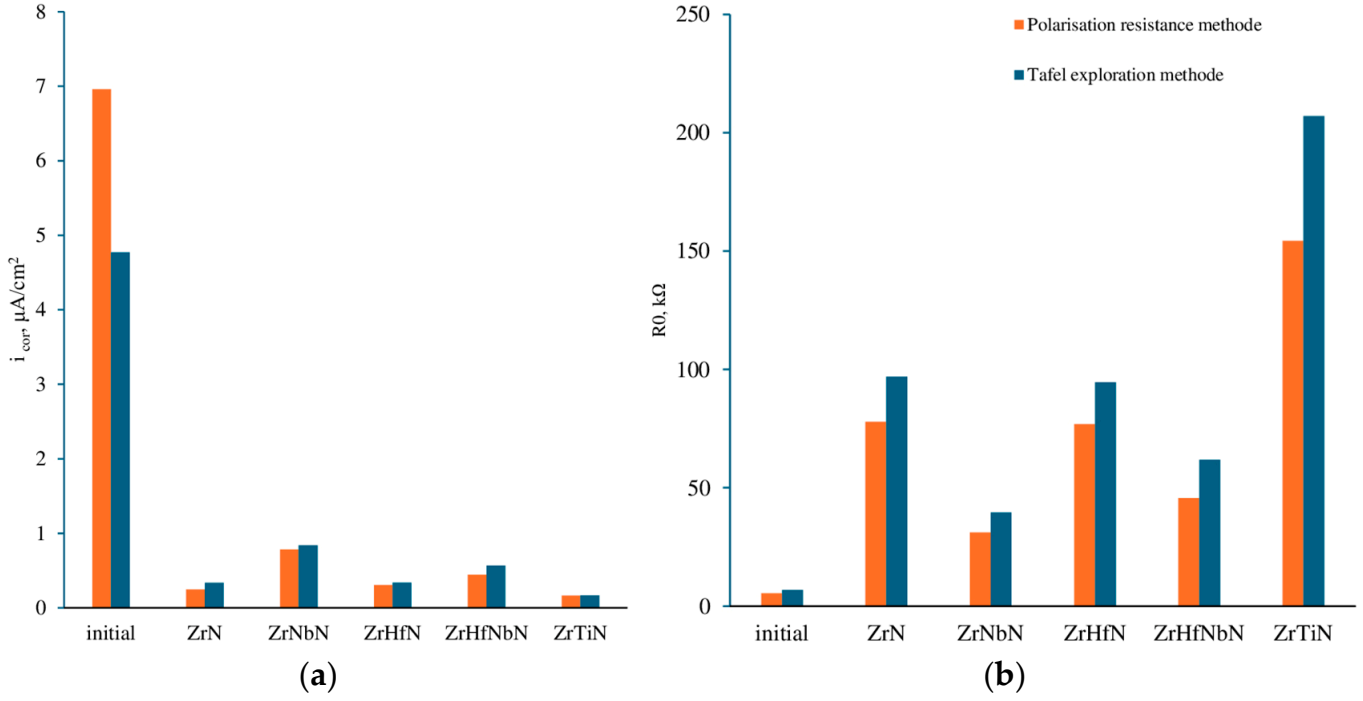

Figure 4. Comparative diagrams for the (**a**) corrosion current density and (**b**) polarisation resistance obtained for AISI 321 steel with different nitride coatings exposed to 3% NaCl at 25 °C.

The structure of this error includes the initially different degree of surface oxidation for two identical samples and, consequently, different primary oxidation rates of coatings during the studies, as well as the non-equilibrium of the processes caused by the flow of corrosion current in the system [38,57].

For subsequent evaluations of the corrosion resistance, the data obtained based on the polarisation resistance in the corrosion potential region (Table 3) were used. However, the corrosion behaviour of uncoated AISI 321 steel in a 3% aqueous NaCl solution at 25 °C is well-characterised using the Tafel equation, with a fairly high corrosion current of 6.96 μA/cm^2.

The high corrosion resistance of AISI 321 steel samples with Zr-(Zr,Ti)N, Zr-ZrN, and Zr-(Zr,Hf)N coatings in 3% NaCl at 25 °C is characterised by relatively low corrosion current densities (0.17–0.34 μA/cm^2) and high polarisation resistances (76.9–154.4 kΩ cm^2), which is over an order of magnitude higher than the polarisation resistance of uncoated AISI 321 steel (6.9 kΩ cm^2). The performance of the Zr-(Zr,Ti)N, Zr-ZrN, Zr-(Zr,Hf)N coatings is primarily ascribed to the presence of a Zr O_2 transition layer, which blocks the spread of corrosion deep into the coating. Samples with a Zr-(Zr,Ti)N coating demonstrate the lowest corrosion currents, namely 0.17 μA/cm^2, owing to the faster dissolution of TiN and the formation of a poorly soluble titanium oxide of non-stoichiometric composition on the surface [38,58], expressed as follows:

$$2TiN + 2yH_2O \longrightarrow 2TiNxOy + (1 - x)\, N_2 + 4yH^+ + 4ye^- \quad (4)$$

$$2TiN_xO_y + 2H_2O \longrightarrow 2Ti^{3+} + (y + 1)\, O_2 + xN_2 + 4H^+ + 10e^- \quad (5)$$

$$Ti^{3+} + xH_2O \longrightarrow TiO_x + 2xH^+ + (2x - 3)\, e^- \quad (6)$$

The introduction of Hf into the coating does not lead to a significant change in corrosion resistance because the ZrO_2 and HfO_2 oxides that form during corrosion have similar chemical properties [56].

The introduction of niobium (Nb) into the coating slightly increased the corrosion current densities to 0.84 and 0.57 μA/cm^2 for Zr,Nb-(Zr,Nb)N and Zr,Hf-(Zr,Hf,Nb)N, respectively. This is due to the dissolution of NbN and the formation of a complex oxide (NbO_x) with a non-stoichiometric composition, which has increased solubility in water because of the acid–base interaction [59,60]. In this case, partial destruction of the NbO_x corrosion product layer and the development of a corrosion process within the transition layer of Zr and Nb are expected.

3.4. Elemental Distribution on the Surface of Coated Samples After Corrosion Exposure

Elemental mapping of the coated specimen surfaces after corrosion testing (Figure 5) reveals some differences in O intensity. Considering that all the coatings contain Zr, this element was chosen as an indicator of the presence of a coating in the 25 μm × 25 μm sample surface area under observation. Accordingly, the O content primarily indicates oxidation processes on the coating surface. The highest O intensity is observed for the Zr,Nb-(Zr,Nb)N and Zr,Hf-(Zr,Hf,Nb)N coatings (i.e., coatings containing Nb). These results correlate well with the data obtained above.

3.4.1. Coating ZrN

XRD shows that peaks from the fcc Fe phase (A1) are more prominent in the substrate (Figure 6). SAED shows that the structure closer to the substrate edge is more dispersed. This is also evident in the images. The number of phases, according to SAED, is approximately equal.

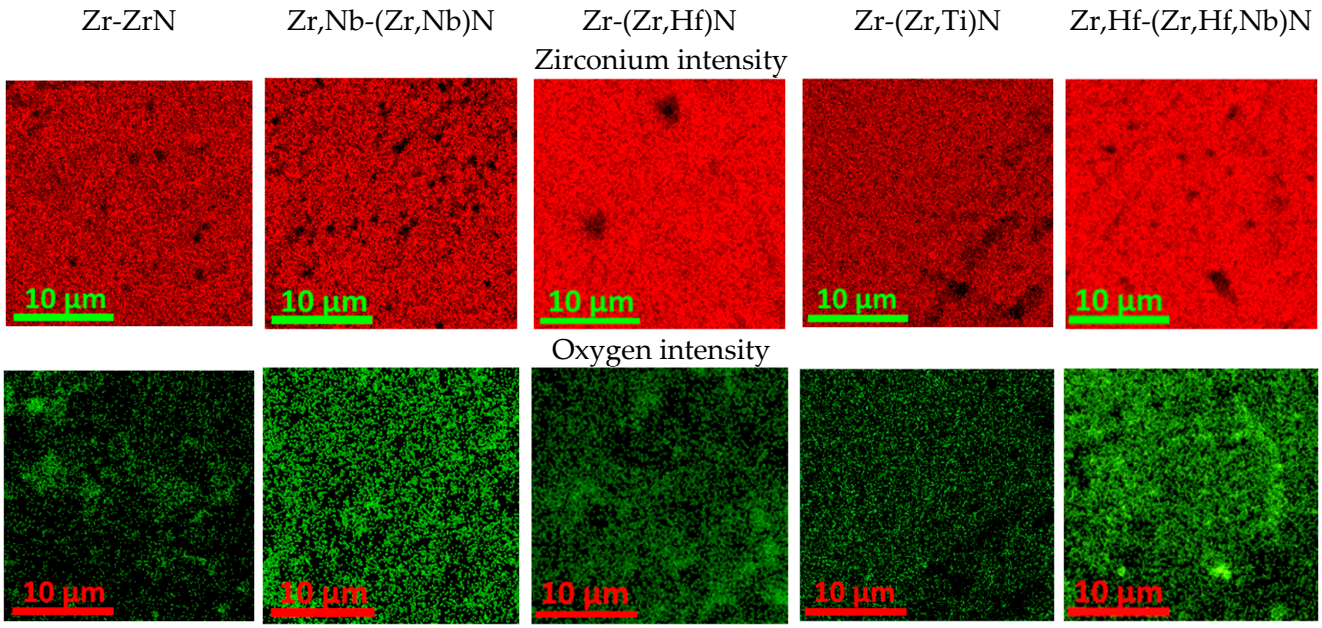

Figure 5. Intensity of the Zr and O distribution in local areas of the coated AISI 321 steel samples after exposure to 3% NaCl solution at 25 °C for 7 days (equivalent surface areas of 25 µm × 25 µm).

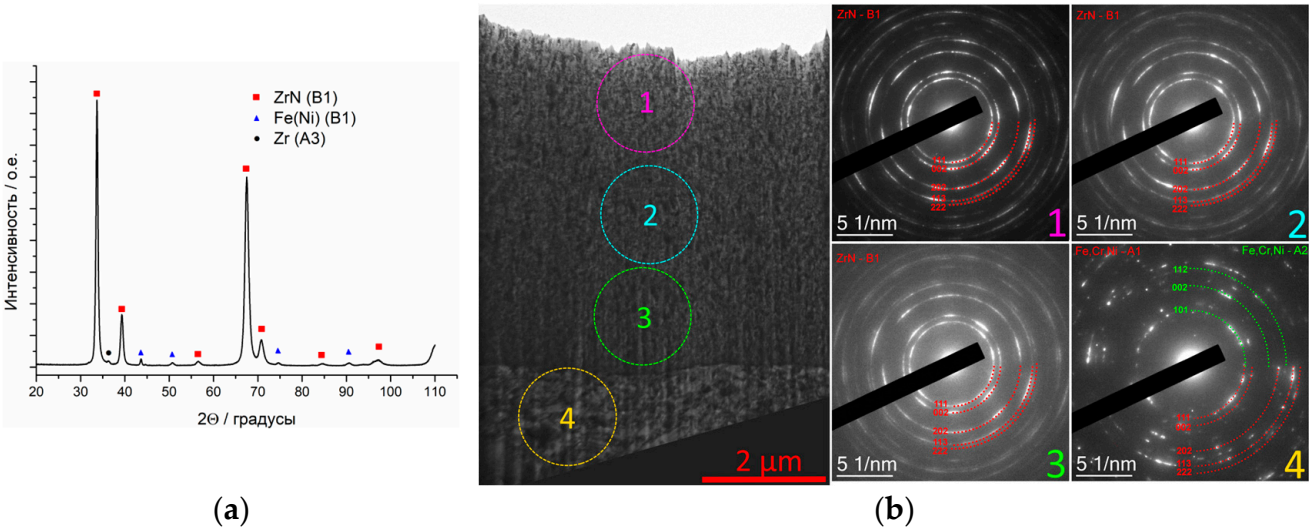

(**a**) (**b**)

Figure 6. (**a**) XRD and (**b**) SAED analyses of a Zr-ZrN-coated sample.

3.4.2. Coating Zr,Hf-(Zr,Hf)N

XRD analysis of the Zr,Hf-(Zr,Hf)N coating shows (Figure 7) that the substrate has more intense peaks from the bcc Fe phase (A1). SAED leads to the same conclusion, indicating that the A1 phase is predominant. The structural dispersion, as seen from both the images and SAED, is significantly lower on the surface of the sample than in the bulk.

From the EDX data, a decrease in Cr content is observed closer to the substrate surface (Figure 8). On the coating surface, the presence of iron oxide particles is noticeable (based on the O and Fe content), but there are no signs of significant oxidation in the coating. At the same time, in some measurement areas (area 2 in Figure 8a–c), both O and the coating elements are present, which indicates the potential formation of zirconium oxides, oxynitrides, and hafnium oxides.

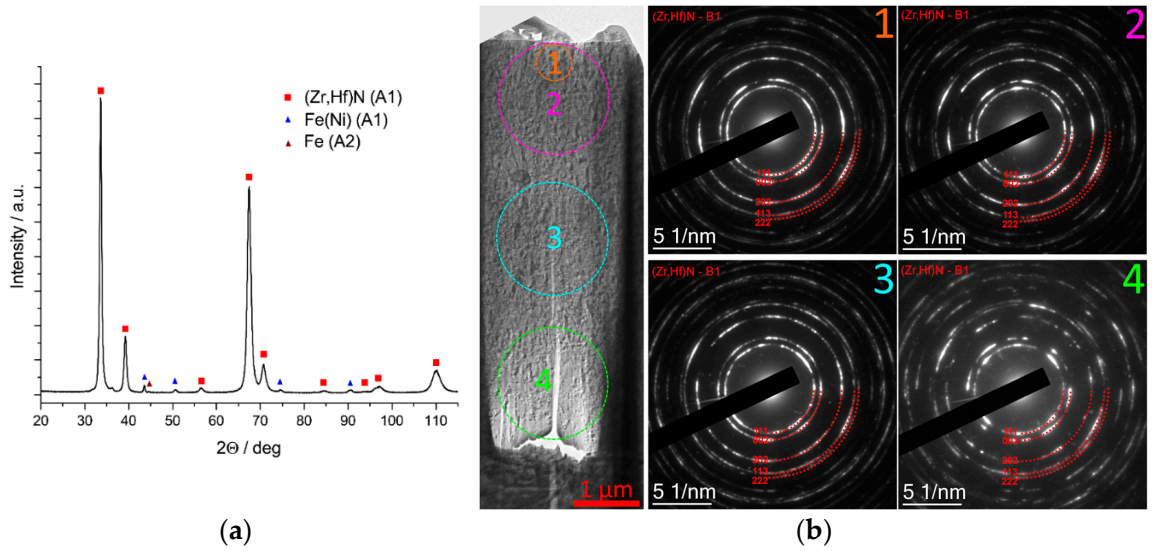

Figure 7. (**a**) XRD and (**b**) SAED analyses of a Zr,Hf-(Zr,Hf)N-coated sample.

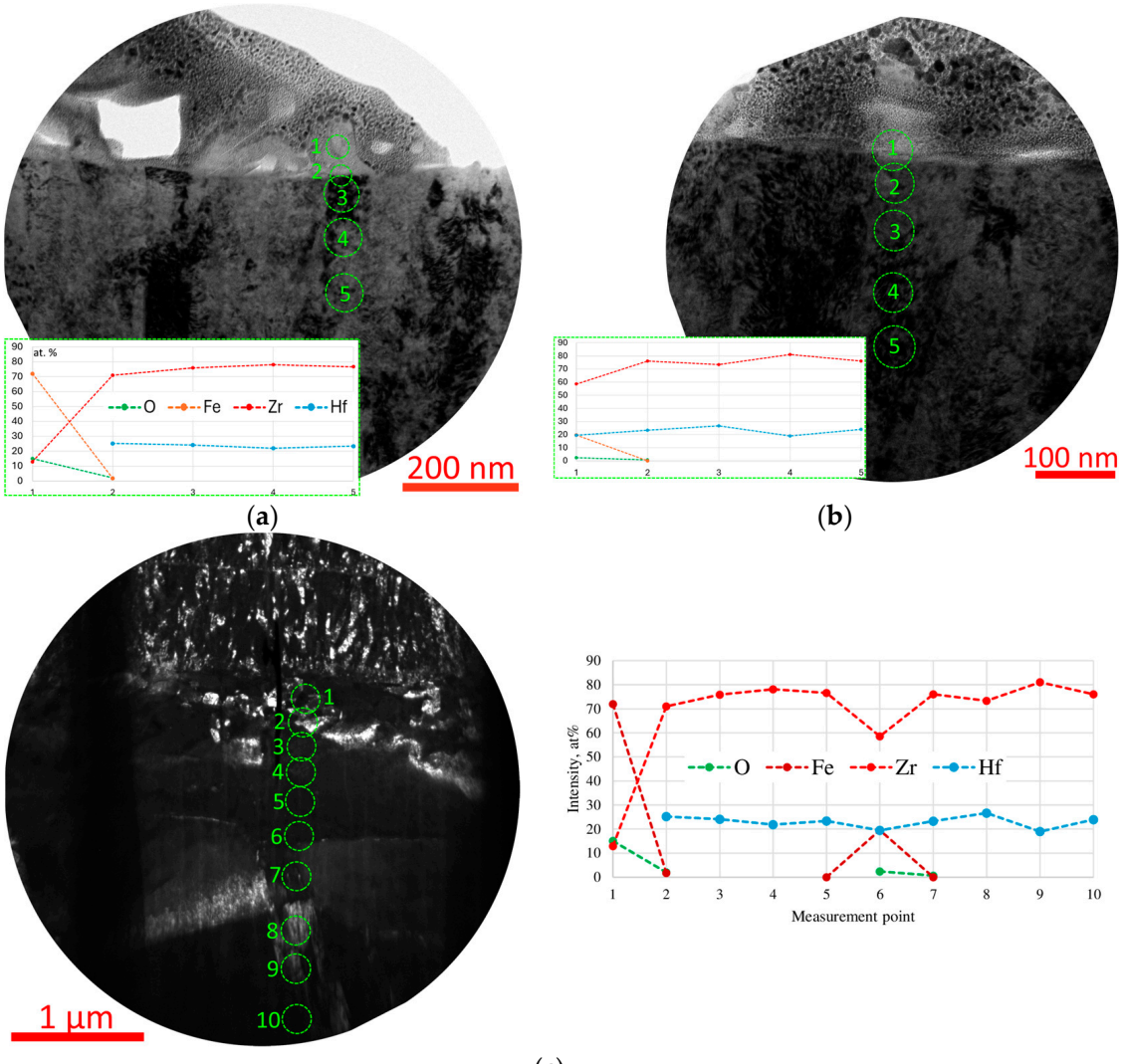

Figure 8. (**a**–**c**) EDX analysis of the elemental distributions in the outer layers of the Zr,Hf-(Zr,Hf)N coating after corrosion testing.

3.4.3. Coating Zr-(Ti,Zr)N

XRD data show that the substrate exhibits more noticeable peaks from the bcc Fe phase (A1) (Figure 9). From the SAED results, it is evident that the structure closer to the edge of the substrate is more dispersed. This is even more noticeable in the images. Consistent with XRD, the bcc Fe phase (A1) is predominant, according to SAED.

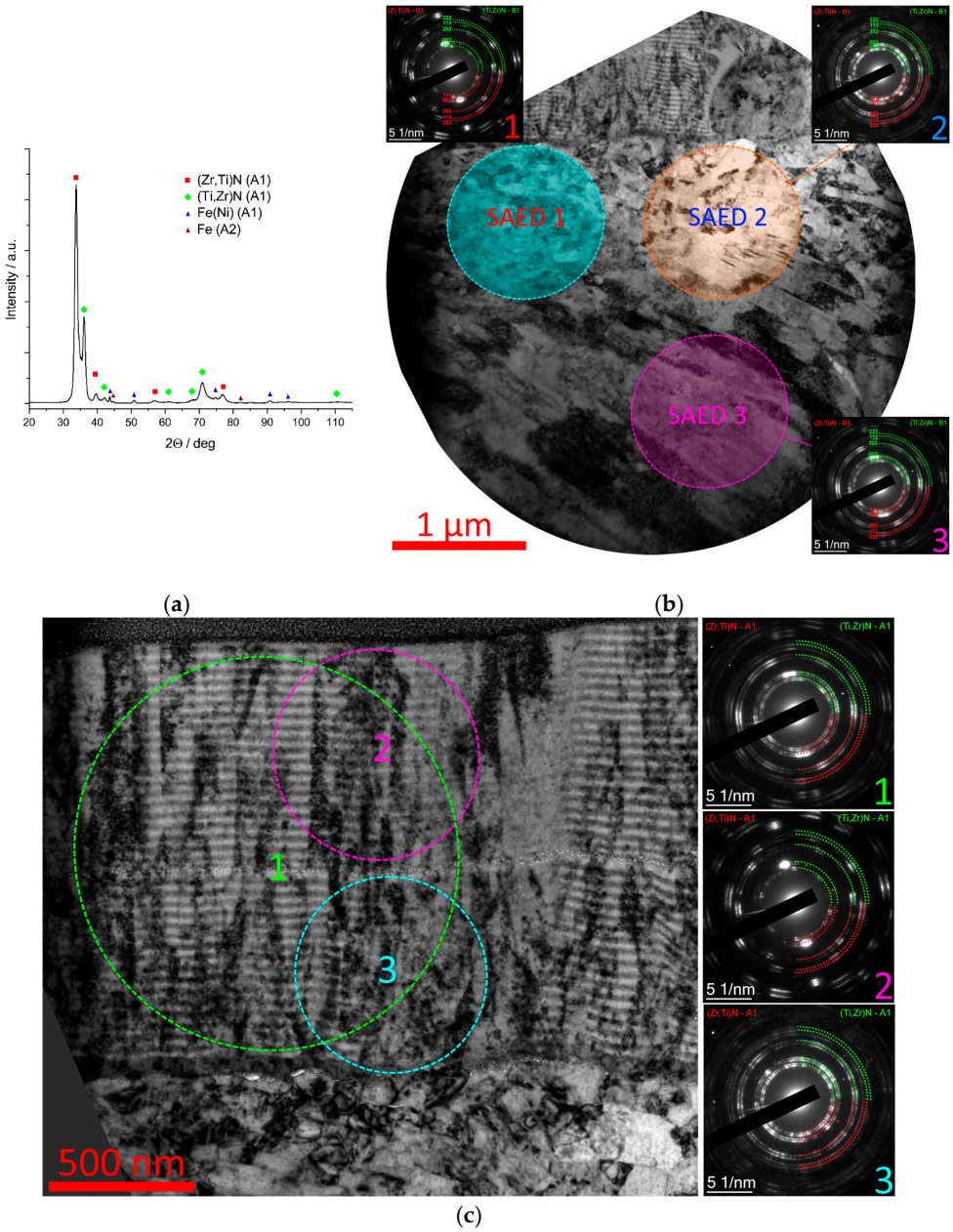

Figure 9. (**a**) XRD and (**b**,**c**) SAED analyses of the phase composition in the (**b**) substrate and (**c**) Zr-(Ti,Zr)N coating.

3.4.4. Coating Zr,Nb-(Zr,Nb,Hf)N

XRD reveals that the amount of bcc Fe (A1) is significantly greater than that of the fcc phase (Figure 10). Based on the SAED reflections, the A2 phase is more abundant than A1 closer to the edge of the substrate, but at greater depth, the A1 phase dominates. The structural dispersion does not change within the visible range of the substrate, as confirmed by SAED. Despite signs of surface oxidation in the coating in the elemental mapping, TEM

studies did not reveal an oxide layer. This layer may be too thin, or it may have been destroyed during lamella preparation.

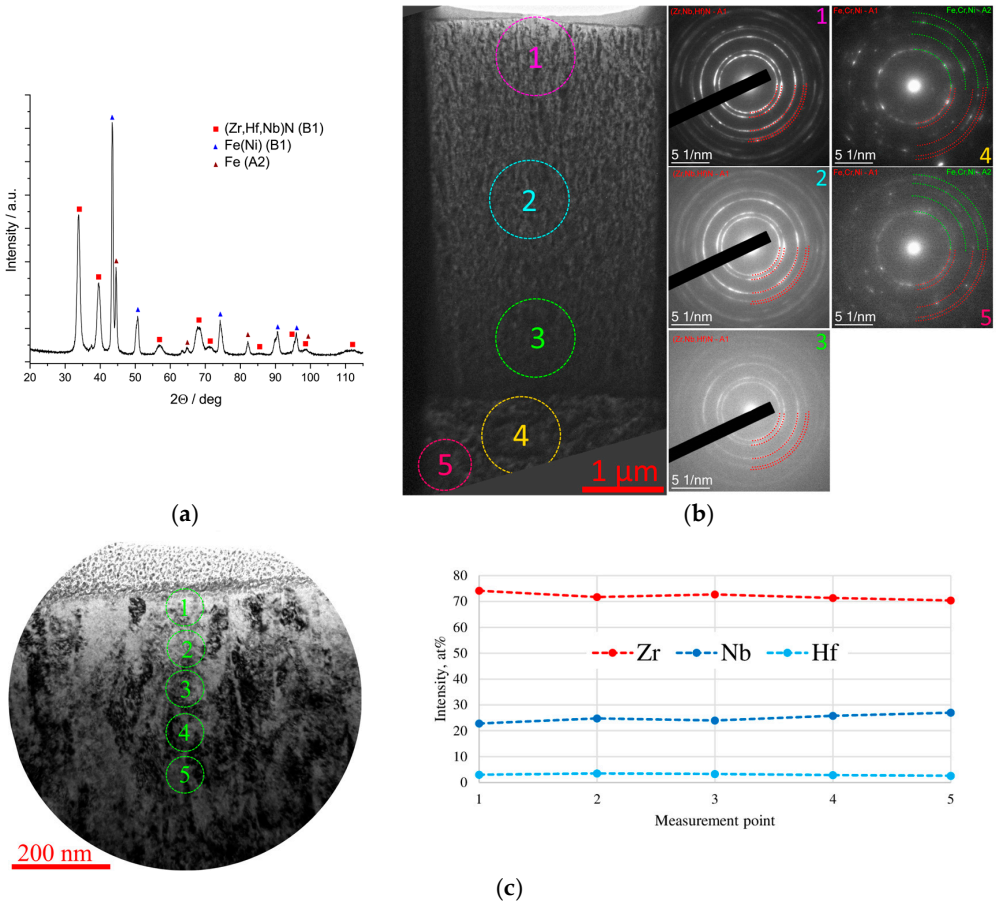

Figure 10. (**a**) XRD, (**b**) SAED, and (**c**) EDX analyses of the phase composition in the Zr-(Ti,Zr)N-coated sample.

3.4.5. Coating Zr,Nb-(Zr,Nb)N

XRD data show that the amount of bcc Fe phase (A1) is higher than that of the fcc phase (Figure 11). This is consistent with the SAED reflections, showing that there is more bcc A1 phase closer to the surface. The structure's dispersion changes towards the edge of the substrate.

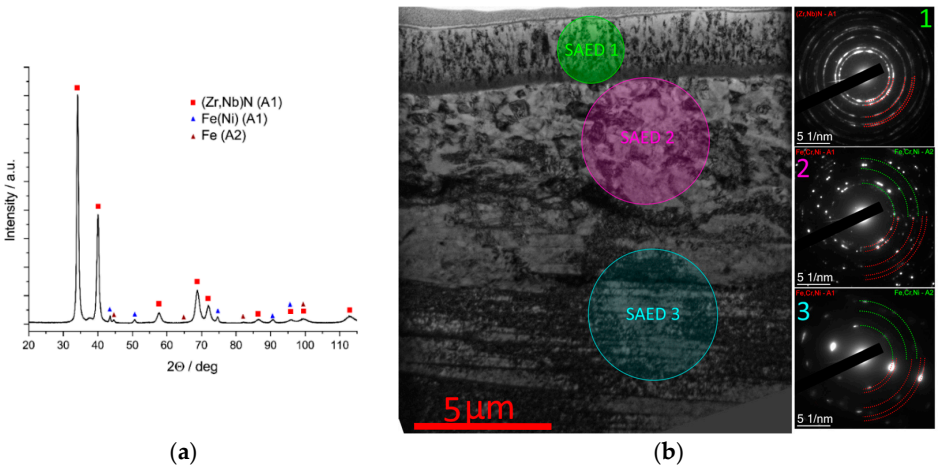

Figure 11. (**a**) XRD and (**b**) SAED analyses of a Zr,Nb-(Zr,Nb)N-coated sample.

4. Discussion

The anticorrosive properties of coated samples are largely related to the adhesion strength between the coating and the substrate. Additionally, the features of the interface between the steel substrate and the coatings with different compositions must be considered. Previous studies on the properties of coatings deposited on a steel substrate show the presence of a transition zone between the coating and the substrate, formed as a result of diffusion and the action of high-energy ions, inducing the mixing of elements in the interfacial zone [61–64]. When the coating peels off from the substrate, an aggressive environment can penetrate the resulting cavities, and active corrosion of the substrate begins [65,66]. In turn, the strength of the adhesive bond between the coating and the substrate is largely determined by the properties of the substrate (e.g., grain size, phases, hardness, and surface roughness) [67–71]. In particular, a decrease in the surface roughness of the stainless steel substrate leads to increased coating adhesion [69] and increased resistance to corrosion in alkaline environments [65]. The residual stress gradient at the coating–substrate interface and defects on the substrate surface significantly affect the performance and failure mode of the coating. The coating wear rate can increase by up to 72% owing to an increase in interface roughness [72]. Laser-modified interfaces significantly reduce the grain size of deposited coatings, weaken their crystallographic texture, and reduce residual stresses, which leads not only to increased adhesion but also to increased corrosion resistance [70]. A similar effect is achieved by plasma [73] and plasma-laser [71] texturing of the substrate before coating deposition. The adhesion strength at the coating–substrate interface also depends on the type of interatomic bonds and the load-bearing capacity of the substrate (hardness), as well as the strength of the outer layers of the substrate [74]. The presence of coating defects is associated with substrate roughness values, with the number of surface defects being a key parameter influencing the rate of coating wear [72]. Furthermore, surface coating defects serve as sites of stress concentration, leading to premature failure of the coating during operation.

In the samples studied herein, a sufficiently tight interface between the coatings and the substrate is observed, with no signs of delamination (Figure 12). The Zr,Nb-(Zr,Nb)N coating exhibits the highest resistance to destruction in the scratch test, whereas the Zr-(Ti,Zr)N, Zr,Hf-(Zr,Hf)N, and Zr,Nb-(Zr,Nb,Hf)N coatings exhibit relatively low fracture strength. At the same time, the Zr,Hf-(Zr,Hf,Nb)N coating provides the best wear resistance and the lowest friction coefficient in the ball-on-disk test, which has previously been established [56]. Thus, the Zr-(Ti,Zr)N coating, although not providing the highest adhesion to the substrate, provides the highest resistance to corrosion. In this case, it can be assumed that the key to corrosion resistance is the non-porous structure of the applied multilayer coatings, in which dense surface films of zirconium oxides and oxonitrides play the primary corrosion-protective role. The addition of Ti nitride to Zr-ZrN significantly decreases the corrosion current density. The introduction of Nb, however, increases the corrosion rate and reduces the polarisation resistance to corrosion, whereas Hf has no effect on the corrosion-protective properties of the nitride coatings. Although the surface oxide layer can only be directly observed in the sample coated with Zr,Hf-(Zr,Hf)N, it may also be present in other samples, based on the elemental mapping data. Further investigation is needed to achieve a more pronounced oxide layer, potentially by increasing the sample soak time in the saline solution and raising the experimental temperature, thereby allowing for a more detailed study.

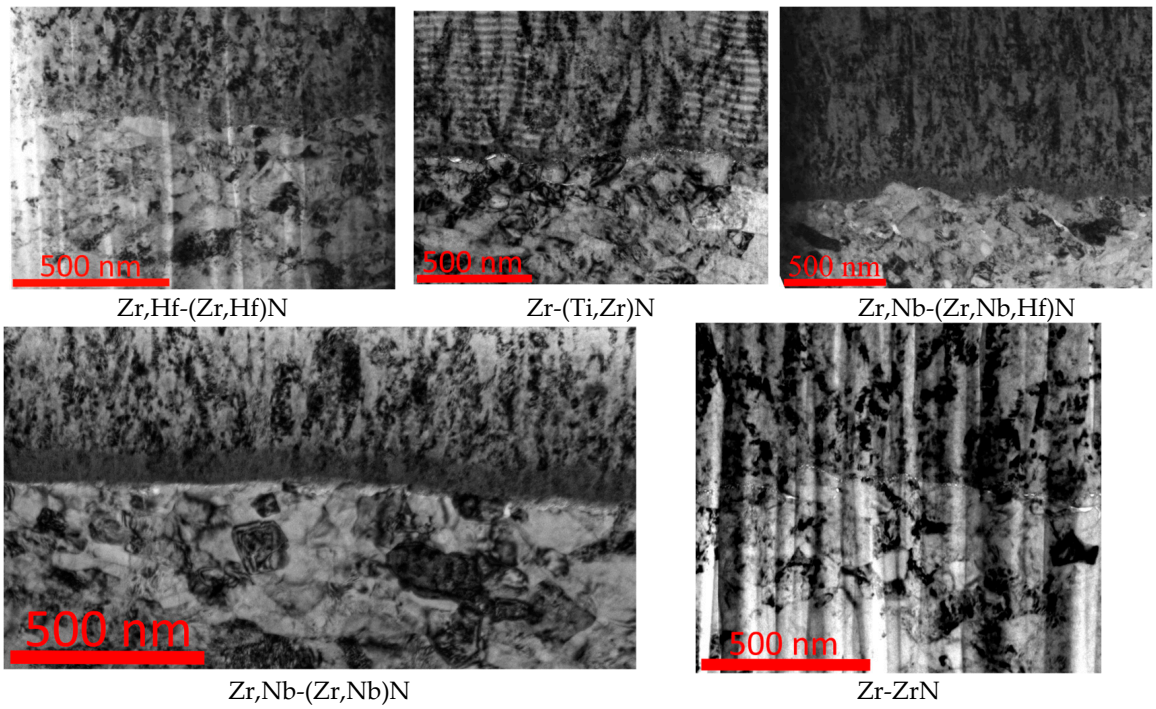

Figure 12. SEM images of the interfaces between the coatings and the substrates in the studied samples.

5. Conclusions

The anticorrosive properties of coatings based on the ZrN system were studied herein, specifically for Zr-(Zr,Hf)N, Zr-(Zr,Ti)N, Zr,Hf-(Zr,Hf,Nb)N, and Zr,Nb-(Zr,Nb)N deposited on AISI 321 stainless steel substrates. The experiments revealed the following findings:

- The (Zr,Hf)N coating had the highest hardness, and the (Zr,Nb)N coating had the lowest hardness. The (Zr,Nb)N coating demonstrated the highest adhesion strength to the substrate (based on the total coating failure rate, L_{C2}), and the ZrN coating also demonstrated a high L_{C2} value, whereas the other coatings demonstrated relatively low values.
- The Zr-ZrN, Zr,Nb-(Zr,Nb)N, Zr-(Zr,Hf)N, Zr,Hf-(Zr,Hf,Nb)N, and Zr-(Zr,Ti)N coatings provided a 10-fold reduction in the corrosion current density in a 3% aqueous NaCl solution at 25 °C, decreasing from 6.96 for the uncoated AISI 321 steel to 0.17 $\mu A/cm^2$ for the Zr-(Zr,Ti)N-coated sample.
- The addition of titanium to ZrN resulted in a significant decrease in corrosion current densities from 0.34 to 0.17 $\mu A/cm^2$, which may be due to the formation of poorly soluble titanium oxide TiO_2 on the surface. However, the addition of Nb increased the corrosion rate and reduced the polarisation resistance to corrosion. This may be due to the formation during corrosion of a non-stoichiometric composition of complex oxides NbO_x with increased solubility in water due to the acid–base interaction. Hf did not affect the corrosion-protective properties of the nitride coatings.
- Although the presence of a surface oxide layer was directly observed only in the Zr,Hf-(Zr,Hf)N-coated sample, it was likely present in the other samples. Further research is necessary to achieve a more pronounced oxide layer, allowing for more detailed investigation.
- Although the Zr,Hf-(Zr,Hf,Nb)N coating provided the best wear resistance and the lowest friction coefficient in the ball-on-disk test, consistent with previous work [56], this coating is not preferred for corrosion protection. In terms of corrosion resistance, the highest performance was provided by the Zr-(Zr,Ti)N, Zr-ZrN, and Zr-(Zr,Hf)N

coatings. Thus, in terms of both high corrosion resistance and high wear resistance, the Zr-(Zr,Hf)N coating is recommended. In the absence of noticeable mechanical wear, the Zr-(Zr,Ti)N coating is the most appropriate for corrosion protection in NaCl solutions (e.g., seawater).

Author Contributions: Conceptualization, A.V. and V.Z.; Methodology, M.V., A.V., C.S., V.Z., A.K. and F.M.; Resources, S.G.; Data curation, S.G., C.S., M.V., T.B., A.T. and A.K.; investigation, C.S., E.E., F.M., T.B.; Supervision, S.G., A.V. and A.T.; Writing—original draft preparation, A.V.; Writing—review and editing, A.V. and C.S.; Project administration, A.V., M.V. and C.S. All authors have read and agreed to the published version of the manuscript.

Funding: This work was funded by the state assignment of the Ministry of Science and Higher Education of the Russian Federation within the framework of the state assignment in the field of scientific activity (project No. FSFS-2023-0003).

Institutional Review Board Statement: Not applicable.

Informed Consent Statement: Not applicable.

Data Availability Statement: The original contributions presented in the study are included in the article; further inquiries can be directed to the corresponding author.

Conflicts of Interest: The authors declare no conflicts of interest.

References

1. Wiiala, U.K.; Penttinen, I.M.; Korhonen, A.S.; Aromaa, J.; Ristolainen, E. Improved corrosion resistance of physical vapour deposition coated TiN and Zr-ZrN. *Surf. Coat. Technol.* **1990**, *41*, 191–204. [CrossRef]
2. Brown, R.; Alias, M.N.; Fontana, R. Effect of composition and thickness on corrosion behavior of TiN and Zr-ZrN thin films. *Surf. Coat. Technol.* **1993**, *62*, 467–473. [CrossRef]
3. Lei, Z.; Zhang, Q.; Zhu, X.; Ma, D.; Ma, F.; Song, Z.; Fu, Y.Q. Corrosion performance of Zr-ZrN/ZrO_2 multilayer coatings deposited on 304 stainless steel using multi-arc ion plating. *Appl. Surf. Sci.* **2018**, *431*, 170–176. [CrossRef]
4. Chou, W.-J.; Yu, G.P.; Huang, J.-H. Corrosion resistance of Zr-ZrN films on AISI 304 stainless steel substrate. *Surf. Coat. Technol.* **2003**, *167*, 59–67. [CrossRef]
5. Yi, P.; Zhu, L.; Dong, C.; Xiao, K. Corrosion and interfacial contact resistance of 316L stainless steel coated with magnetron sputtered Zr-ZrN and TiN in the simulated cathodic environment of a proton-exchange membrane fuel cell. *Surf. Coat. Technol.* **2019**, *363*, 198–202. [CrossRef]
6. Dur, E.; Cora, Ö.N.; Koç, M. Effect of manufacturing process sequence on the corrosion resistance characteristics of coated metallic bipolar plates. *J. Power Sources* **2014**, *246*, 788–799. [CrossRef]
7. Lin, M.-T.; Wan, C.-H.; Wu, W. Enhanced corrosion resistance of SS304 stainless steel and titanium coated with alternate layers of TiN and Zr-ZrN in a simulated O_2-rich environment of a unitized regenerative fuel cell. *Int. J. Electrochem. Sci.* **2014**, *9*, 7832–7845. [CrossRef]
8. Lin, Y.-W.; Huang, J.-H.; Yu, G.-P. Microstructure and corrosion resistance of nanocrystalline TiZr-ZrN films on AISI 304 stainless steel substrate. *J. Vac. Sci. Technol. A Vac. Surf. Film.* **2010**, *28*, 774–778. [CrossRef]
9. Xi, Y.; Wan, L.; Hou, J.; Wang, Z.; Wang, L.; Yang, D.; Liu, D.; Lei, S. Improvement of erosion-corrosion behavior of AISI 420 stainless steel by ion-assisted deposition Zr-ZrN coatings. *Metals* **2021**, *11*, 1811. [CrossRef]
10. Das Mercês Reis De Castro, M.; Ferreira, C.P.; Da Silva, B.P.; Tentardini, E.K.; De Freitas Cunha Lins, V. Corrosion performance evaluation of Zr-ZrN and ZrSiN coatings deposited on steel surface by magnetron sputtering. *Eur. Corros. Congr. Eurocorr.* **2016**, *2*, 1417–1424.
11. Ferreira, C.P.; Castro, M.D.M.R.D.; Tentardini, E.K.; Lins, V.D.F.C.; Saliba, P.A. Silicon influence on corrosion resistance of magnetron sputtered Zr-ZrN and ZrSiN thin films. *Surf. Eng.* **2020**, *36*, 33–40. [CrossRef]
12. Zhang, Z.; Chen, M.; Gyawali, G.; Zhang, T.F.; Zhang, S. Effect of nitrogen pressure on the microstructure, conductivity, and corrosion resistance of Zr-ZrN-coated stainless steel as bipolar plate for proton exchange membrane fuel cell. *Ceram. Int.* **2024**, *50*, 44678–44688. [CrossRef]
13. Huang, J.-H.; Hsu, C.-Y.; Chen, S.-S.; Yu, G.-P. Effect of substrate bias on the structure and properties of ion-plated Zr-ZrN on Si and stainless steel substrates. *Mater. Chem. Phys.* **2003**, *77*, 14–21. [CrossRef]
14. Huang, J.-H.; Kuo, K.-L.; Yu, G.-P. Oxidation behavior and corrosion resistance of vacuum annealed Zr-ZrN-coated stainless steel. *Surf. Coat. Technol.* **2019**, *358*, 308–319. [CrossRef]

15. Samim, P.M.; Fattah-Alhosseini, A.; Elmkhah, H.; Imantalab, O. A study on the corrosion resistance of Zr-ZrN/CrN multilayer nanostructured coating applied on AISI 304 stainless steel using Arc-PVD method in 3.5 wt% NaCl solution. *Mater. Res. Express* **2019**, *6*, 126426. [CrossRef]
16. Mohamadian Samim, P.; Fattah-Alhosseini, A.; Elmkhah, H.; Imantalab, O. Structure and corrosion behavior of Zr-ZrN/CrN nano-multilayer coating deposited on AISI 304 stainless steel by CAE-PVD technique. *J. Asian Ceram. Soc.* **2020**, *8*, 460–469. [CrossRef]
17. Guan, X.; Zhao, M.; Shi, H.; Wang, Y.; Wang, Z.; Cheng, Y.; Liu, M. CrZr-ZrN/Zr-ZrN multilayer coatings on 316L stainless steel towards anticorrosion application. *Thin Solid Film.* **2022**, *755*, 139330. [CrossRef]
18. Rajabi, T.; Atapour, M.; Elmkhah, H.; Nahvi, S.M. Nanometric CrN/CrAlN and CrN/Zr-ZrN multilayer physical vapor deposited coatings on 316L stainless steel as bipolar plate for proton exchange membrane fuel cells. *Thin Solid Film.* **2022**, *753*, 139288. [CrossRef]
19. De Sánchez, N.A.; Jaramillo, H.E.; Vivas, Z.; Aperador, W.; Amaya, C.; Caicedo, J.C. Fracture resistant and wear corrosion performance of CrN/Zr-ZrN bilayers deposited onto AISI 420 stainless steel. *Adv. Mater. Res.* **2008**, *38*, 63–75. [CrossRef]
20. Barshilia, H.C.; Prakash, M.S.; Poojari, A.; Rajam, K.S. Corrosion behavior of nanolayered TiN/NbN multilayer coatings prepared by reactive direct current magnetron sputtering process. *Thin Solid Film.* **2004**, *460*, 133–142. [CrossRef]
21. Subramanian, B. Enhancement of biocompatibility of metal implants by nanoscale TiN/NbN multilayer coatings. *J. Nanosci. Nanotechnol.* **2013**, *13*, 4565–4572. [CrossRef]
22. Barshilia, H.C.; Rajam, K.S. Structure and properties of reactive DC magnetron sputtered TiN/NbN hard superlattices. *Surf. Coat. Technol.* **2004**, *183*, 174–183. [CrossRef]
23. Purandare, Y.P.; Stack, M.M.; Hovsepian, P.E. Velocity effects on erosion-corrosion of CrN/NbN superlattice PVD coatings. *Surf. Coat. Technol.* **2006**, *201*, 361–370. [CrossRef]
24. Chen, J.; Zhang, S.; Li, J.; Chen, Z.; Sun, D. Effects of phase transformation on the corrosion resistance and conductivity of NbN coatings for metal bipolar plates. *Surf. Coat. Technol.* **2025**, *497*, 131800. [CrossRef]
25. Monticelli, C.; Balbo, A.; Zucchi, F. Corrosion and tribocorrosion behaviour of cermet and cermet/nanoscale multilayer CrN/NbN coatings. *Surf. Coat. Technol.* **2010**, *204*, 1452–1460. [CrossRef]
26. Purandare, Y.; Stack, M.M.; Hovsepian, P. A study of the erosion-corrosion of PVD CrN/NbN superlattice coatings in aqueous slurries. *Wear* **2005**, *259*, 256–262. [CrossRef]
27. Hovsepian, P.E.; Lewis, D.B.; Luo, Q.; Farinotti, A. Corrosion resistance of CrN/NbN superlattice coatings grown by various physical vapour deposition techniques. *Thin Solid Film.* **2005**, *488*, 1–8. [CrossRef]
28. Hovsepian, P.E.; Lewis, D.B.; Münz, W.D.; Lyon, S.B.; Tomlinson, M. Combined cathodic arc/unbalanced magnetron grown CrN/NbN superlattice coatings for corrosion resistant applications. *Surf. Coat. Technol.* **1999**, *120–121*, 535–541. [CrossRef]
29. Lewis, D.B.; Creasey, S.J.; Wüstefeld, C.; Ehiasarian, A.P.; Hovsepian, P.E. The role of the growth defects on the corrosion resistance of CrN/NbN superlattice coatings deposited at low temperatures. *Thin Solid Film.* **2006**, *503*, 143–148. [CrossRef]
30. Chen, M.; Ding, J.C.; Kwon, S.-H.; Wang, Q.; Zhang, S. Corrosion resistance and conductivity of NbN-coated 316L stainless steel bipolar plates for proton exchange membrane fuel cells. *Corros. Sci.* **2022**, *196*, 110042. [CrossRef]
31. Carvalho, R.G.; Fonseca, R.M.; Lins, V.D.F.C.; Castro, M.D.M.R.D.; Tentardini, E.K. Corrosion resistance of NbN and Nb_xAl_yN coatings on stainless steel. *Surf. Eng.* **2021**, *37*, 1579–1585. [CrossRef]
32. Huang, W.; Zalnezhad, E.; Musharavati, F.; Jahanshahi, P. Investigation of the tribological and biomechanical properties of CrAlTiN and CrN/NbN coatings on SST 304. *Ceram. Int.* **2017**, *43*, 7992–8003. [CrossRef]
33. Fonseca, R.M.; Soares, R.B.; Carvalho, R.G.; Tentardini, E.K.; Lins, V.F.C.; Castro, M.M.R. Corrosion behavior of magnetron sputtered NbN and $Nb_{1-x}Al_xN$ coatings on AISI 316L stainless steel. *Surf. Coat. Technol.* **2019**, *378*, 124987. [CrossRef]
34. Zhang, D.; Qi, Z.; Wei, B.; Shen, H.; Wang, Z. Microstructure and corrosion behaviors of conductive Hf/HfN multilayer coatings on magnesium alloys. *Ceram. Int.* **2018**, *44*, 9958–9966. [CrossRef]
35. Escobar, C.; Villarreal, M.; Caicedo, J.C.; Aperador, W.; Prieto, P. Novel performance in physical and corrosion resistance HfN/VN coating system. *Surf. Coat. Technol.* **2013**, *221*, 182–190. [CrossRef]
36. Bian, S.; Chen, C.; Yu, L.; Lu, G.; Xu, J. Improvement of structures and properties of hafnium nitride coatings by yttrium introduction. *Surf. Coat. Technol.* **2024**, *478*, 130358. [CrossRef]
37. He, T.; Valery, Z.; Vereschaka, A.; Keshin, A.; Huo, Y.; Milovich, F.; Sotova, C.; Seleznev, A. Influence of niobium and hafnium doping on the wear and corrosion resistance of coatings based on ZrN. *J. Mater. Res. Technol.* **2023**, *27*, 6386–6399. [CrossRef]
38. Tao, H.; Zhylinski, V.; Vereschaka, A.; Chayeuski, V.; Yuanming, H.; Milovich, F.; Sotova, C.; Seleznev, A.; Salychits, O. Comparison of the Mechanical Properties and Corrosion Resistance of the Cr-CrN, Ti-TiN, Zr-ZrN, and Mo-MoN Coatings. *Coatings* **2023**, *13*, 750. [CrossRef]
39. Takahashi, M.; Kikuchi, M.; Takada, Y.; Okuno, O. Corrosion resistance of dental Ti-Ag alloys in NaCl solution. *Mater. Trans.* **2010**, *51*, 762–766. [CrossRef]

40. Nichul, U.; Tambe, P.; Hiwarkar, V. Electrochemical Behaviour of Textured Beta C Titanium Alloy in 3.5% NaCl Solution. *Arch. Metall. Mater.* **2024**, *69*, 571–577. [CrossRef]
41. Wang, H.; Wang, J.; Peng, X.; Shan, C. Corrosion behavior of three titanium alloys in 3.5%NaCl solution. *J. Chin. Soc. Corros. Prot.* **2015**, *35*, 75–80.
42. Grigoriev, S.; Volosova, M.; Zhylinski, V.; Sotova, C.; Milovich, F.; Seleznev, A.; Pianka, H.; Makarevich, K.; Potapov, P.; Vereschaka, A. Increasing the Corrosion Resistance of Austenitic Stainless Steel Products by Depositing Vanadium Nitride-Based Coatings on Their Surface. *J. Compos. Sci.* **2025**, *9*, 498. [CrossRef]
43. Olsson, C.O.A. Passivation of Stainless Steels and Other Chromium Bearing Alloys. In *Encyclopedia of Interfacial Chemistry Surface Science and Electrochemistry*; Wandelt, K., Ed.; Elsevier Inc.: Amsterdam, The Netherlands, 2018; pp. 357–364.
44. Mansfeld, F. The Polarization Resistance Technique for Measuring Corrosion Currents. In *Advances in Corrosion Science and Technology*; Fontana, G., Staehle, R.W., Eds.; Plenum Press: New York, NY, USA, 1976; Volume 6, p. 163.
45. Grigoriev, S.; Vereschaka, A.; Milovich, F.; Sitnikov, N.; Andreev, N.; Bublikov, J.; Kutina, N. Investigation of the properties of the Cr,Mo-(Cr,Mo,Zr,Nb)N-(Cr,Mo,Zr,Nb,Al)N multilayer composite multicomponent coating with nanostructured wear-resistant layer. *Wear* **2021**, *468–469*, 203597. [CrossRef]
46. Vereschaka, A.A.; Bublikov, J.I.; Sitnikov, N.N.; Oganyan, G.V.; Sotova, C.S. Influence of nanolayer thickness on the perfor-mance properties of multilayer composite nano-structured modified coatings for metal-cutting tools. *Int. J. Adv. Manuf. Technol.* **2018**, *95*, 2625–2640. [CrossRef]
47. Grigoriev, S.; Vereschaka, A.; Milovich, F.; Migranov, M.; Andreev, N.; Bublikov, J.; Sitnikov, N.; Oganyan, G. Investigation of the tribological properties of Ti-TiN-(Ti,Al,Nb,Zr)N composite coating and its efficiency in increasing wear resistance of metal cutting tools. *Tribol. Int.* **2021**, *164*, 107236. [CrossRef]
48. Vereschaka, A.S.; Grigoriev, S.N.; Sotova, E.S.; Vereschaka, A.A. Improving the efficiency of the cutting tools made of mixed ceramics by applying modifying nano-scale multilayered coatings. *Adv. Mat. Res.* **2013**, *712–715*, 391–394.
49. Volosova, M.; Grigoriev, S.; Metel, A.; Shein, A. The Role of Thin-Film Vacuum-Plasma Coatings and Their Influence on the Efficiency of Ceramic Cutting Inserts. *Coatings* **2018**, *8*, 287. [CrossRef]
50. Grigoriev, S.N.; Volosova, M.A.; Vereschaka, A.A.; Sitnikov, N.N.; Milovich, F. Properties of (Cr,Al,Si)N-(DLC-Si) composite coatings deposited on a cutting ceramic substrate. *Ceram. Int.* **2020**, *46*, 18241–18255. [CrossRef]
51. Grigoriev, S.; Vereschaka, A.; Milovich, F.; Sitnikov, N.; Seleznev, A.; Sotova, C.; Bublikov, J. Influence of the yttrium cathode arc current on the yttrium content in the (Ti,Y,Al) N coating and the coating properties. *Vacuum* **2024**, *222*, 113028. [CrossRef]
52. Grigoriev, S.; Vereschaka, A.; Zelenkov, V.; Sitnikov, N.; Bublikov, J.; Milovich, F.; Andreev, N.; Sotova, C. Investigation of the influence of the features of the deposition process on the structural features of microparticles in PVD coatings. *Vacuum* **2022**, *202*, 111144. [CrossRef]
53. *ASTM C1624-05*; Standard Test Method for Adhesion Strength and Mechanical Failure Modes of Ceramic Coatings by Quantitative Single Point Scratch Testing. ASTM International: West Conshohocken, PA, USA, 2010. [CrossRef]
54. Poorqasemi, E.; Abootalebi, O.; Peikari, M.; Haqdar, F. Investigating accuracy of the Tafel extrapolation method in HCl solutions. *Corros. Sci.* **2009**, *51*, 1043–1054. [CrossRef]
55. Meija, J.; Coplen, T.B.; Berglund, M.; Brand, W.A.; De Bièvre, P.; Gröning, M.; Holden, N.E.; Irrgeher, J.; Loss, R.D.; Walczyk, T.; et al. Atomic weights of the elements 2013 (IUPAC Technical Report). *Pure Appl. Chem.* **2016**, *88*, 265–291. [CrossRef]
56. Vereschaka, A.A.; Vereschaka, A.S.; Bublikov, J.I.; Aksenenko, A.Y.; Sitnikov, N.N. Study of properties of nanostructured multilayer composite coatings of Ti-TiN-(TiCrAl)N and Zr-ZrN-(ZrNbCrAl)N. *J. Nano Res.* **2016**, *40*, 90–98. [CrossRef]
57. Volosova, M.; Zhylinski, V.; Sotova, C.; Milovich, F.; Seleznev, A.; Pyanka, H.; Makarevich, K.; Vereschaka, A. Features of the Application of Coatings Based on the ZrN System to Increase Resistance to Mechanical Wear and Corrosion of Titanium Alloy Products. *Coatings* **2024**, *14*, 1304. [CrossRef]
58. Roman, D.; Bernardi, J.; de Amorim, C.L.; de Souza, F.S.; Spinelli, A.; Giacomelli, C.; Figueroa, C.A.; Baumvol, I.J.; Basso, R.L. Effect of deposition temperature on microstructure and corrosion resistance of ZrN thin films deposited by DC reactive magnetron sputtering. *Mater. Chem. Phys.* **2011**, *130*, 147–153. [CrossRef]
59. Ma, Z.-K.; Gao, Y.; Cai, H.-W.; Wang, C.; Yuan, L.; Zhang, Y.; Wu, W.-Q. Corrosion resistance of TiN and CrN coatings with arc ion plating on 201 stainless steel surface. *Corros. Prot.* **2013**, *34*, 670–672.
60. Bekermann, D.; Barreca, D.; Gasparotto, A.; Becker, H.W.; Fischer, R.A.; Devi, A. Investigation of niobium nitride and oxy-nitride films grown by MOCVD. *Surf. Coat. Technol.* **2009**, *204*, 404–409. [CrossRef]
61. Lukaszkowicz, K.; Dobrzański, L.A. Structure and mechanical properties of gradient coatings deposited by PVD technology onto the X40CrMoV5-1 steel substrate. *J. Mater. Sci.* **2008**, *43*, 3400–3407. [CrossRef]
62. Lukaszkowicz, K.; Sondor, J.; Kriz, A.; Pancielejko, M. Structure, mechanical properties and corrosion resistance of nanocomposite coatings deposited by PVD technology onto the X6CrNiMoTi17-12-2 and X40CrMoV5-1 steel substrates. *J. Mater. Sci.* **2010**, *45*, 1629–1637. [CrossRef]

63. Grigoriev, S.; Volosova, M.; Sotova, C.; Milovich, F.; Seleznev, A.; Makarevich, K.; Potapov, P.; Vereschaka, A. Increasing the Wear Resistance of Stainless Steel Products by Depositing Modifying Coatings Based on Zirconium Nitride with the Addition of Niobium, Hafnium, and Titanium. *J. Manuf. Mater. Process.* **2025**, *9*, 316. [CrossRef]
64. Lukaszkowicz, K.; Konieczny, J. Microstructure and mechanical properties of PVD nanoncrystalline layer. *Solid State Phenom.* **2012**, *186*, 230–233. [CrossRef]
65. Hu, X.; Liu, S.; Liu, Q.; Su, Y.; Wu, J.; Xie, Z.; Guo, J.; Zhu, W. Effect of interface roughness on the CMAS + molten salt (Na_2SO_4 + NaCl + $NaVO_3$) corrosion resistance of EB-PVD thermal barrier coatings. *Surf. Coat. Technol.* **2025**, *503*, 13202. [CrossRef]
66. Liu, G.; Zhu, W.; Liu, S.; Guo, J.; Ma, Z. Real-time acoustic emission detection of damage mode and failure of EB-PVD thermal barrier coating under CMAS and sea salt corrosion. *J. Eur. Ceram. Soc.* **2025**, *45*, 117404. [CrossRef]
67. Wang, X.; Pei, Y.; Ma, Y. The effect of microstructure at interface between coating and substrate on damping capacity of coating systems. *Appl. Surf. Sci.* **2013**, *282*, 60–66. [CrossRef]
68. Chen, Y.; Zhang, L.; Zhu, J.-F.; Zhong, Z.-Q.; Gu, J.-H. Cohesive failure and film adhesion of PVD coating: Cemented carbide substrate phase effect and its micro-mechanism. *Int. J. Refract. Met. Hard Mater.* **2023**, *111*, 106066. [CrossRef]
69. Tillmann, W.; Hagen, L.; Stangier, D.; Dias, N.F.L.; Görtz, J.; Kensy, M.D. Lapping and polishing of additively manufactured 316L substrates and their effects on the microstructural evolution and adhesion of PVD CrAlN coatings. *Surf. Coat. Technol.* **2021**, *428*, 127905. [CrossRef]
70. Zhang, L.; Xiong, Q.; Jian, Q.; Qiu, X.; Li, C. Effect of laser interface pretreatment on the microstructure, adhesion strength, and corrosion resistance of PVD-AlTiN coatings on Mg alloy substrates. *Surf. Coat. Technol.* **2025**, *516*, 13267. [CrossRef]
71. Meng, X.; Zhang, K.; Guo, X.; Wang, C.; Sun, L. Preparation of micro-textures on cemented carbide substrate surface by plasma-assisted laser machining to enhance the PVD tool coatings adhesion. *J. Mater. Process. Technol.* **2021**, *288*, 116870. [CrossRef]
72. Teles, V.C.; de Mello, J.D.B.; da Silva, W.M. Abrasive wear of multilayered/gradient CrAlSiN PVD coatings: Effect of interface roughness and of superficial flaws. *Wear* **2017**, *376–377*, 1691–1701. [CrossRef]
73. Herrera-Jimenez, E.J.; Bousser, E.; Schmitt, T.; Klemberg-Sapieha, J.E.; Martinu, L. Effect of plasma interface treatment on the microstructure, residual stress profile, and mechanical properties of PVD TiN coatings on Ti-6Al-4V substrates. *Surf. Coat. Technol.* **2021**, *413*, 127058. [CrossRef]
74. Sveen, S.; Andersson, J.M.; M'Saoubi, R.; Olsson, M. Scratch adhesion characteristics of PVD TiAlN deposited on high speed steel, cemented carbide and PCBN substrates. *Wear* **2013**, *308*, 133–141. [CrossRef]